CLNS 04/1860
CLEO 04-02

Measurement of the B-Meson Inclusive Semileptonic Branching Fraction and Electron-Energy Moments

A. H. Mahmood,[1] S. E. Csorna,[2] G. Bonvicini,[3] D. Cinabro,[3] M. Dubrovin,[3] A. Bornheim,[4] E. Lipeles,[4] S. P. Pappas,[4] A. Shapiro,[4] A. J. Weinstein,[4] R. A. Briere,[5] G. P. Chen,[5] T. Ferguson,[5] G. Tatishvili,[5] H. Vogel,[5] M. E. Watkins,[5] N. E. Adam,[6] J. P. Alexander,[6] K. Berkelman,[6] V. Boisvert,[6] D. G. Cassel,[6] J. E. Duboscq,[6] K. M. Ecklund,[6] R. Ehrlich,[6] R. S. Galik,[6] L. Gibbons,[6] B. Gittelman,[6] S. W. Gray,[6] D. L. Hartill,[6] B. K. Heltsley,[6] L. Hsu,[6] C. D. Jones,[6] J. Kandaswamy,[6] D. L. Kreinick,[6] V. E. Kuznetsov,[6] A. Magerkurth,[6] H. Mahlke-Krüger,[6] T. O. Meyer,[6] J. R. Patterson,[6] T. K. Pedlar,[6] D. Peterson,[6] J. Pivarski,[6] D. Riley,[6] A. J. Sadoff,[6] H. Schwarthoff,[6] M. R. Shepherd,[6] W. M. Sun,[6] J. G. Thayer,[6] D. Urner,[6] T. Wilksen,[6] M. Weinberger,[6] S. B. Athar,[7] P. Avery,[7] L. Breva-Newell,[7] V. Potlia,[7] H. Stoeck,[7] J. Yelton,[7] B. I. Eisenstein,[8] G. D. Gollin,[8] I. Karliner,[8] N. Lowrey,[8] P. Naik,[8] C. Sedlack,[8] M. Selen,[8] J. J. Thaler,[8] J. Williams,[8] K. W. Edwards,[9] D. Besson,[10] K. Y. Gao,[11] D. T. Gong,[11] Y. Kubota,[11] S. Z. Li,[11] R. Poling,[11] A. W. Scott,[11] A. Smith,[11] C. J. Stepaniak,[11] J. Urheim,[11] Z. Metreveli,[12] K. K. Seth,[12] A. Tomaradze,[12] P. Zweber,[12] J. Ernst,[13] K. Arms,[14] E. Eckhart,[14] K. K. Gan,[14] C. Gwon,[14] H. Severini,[15] P. Skubic,[15] D. M. Asner,[16] S. A. Dytman,[16] S. Mehrabyan,[16] J. A. Mueller,[16] S. Nam,[16] V. Savinov,[16] G. S. Huang,[17] D. H. Miller,[17] V. Pavlunin,[17] B. Sanghi,[17] E. I. Shibata,[17] I. P. J. Shipsey,[17] G. S. Adams,[18] M. Chasse,[18] J. P. Cummings,[18] I. Danko,[18] J. Napolitano,[18] D. Cronin-Hennessy,[19] C. S. Park,[19] W. Park,[19] J. B. Thayer,[19] E. H. Thorndike,[19] T. E. Coan,[20] Y. S. Gao,[20] F. Liu,[20] R. Stroynowski,[20] M. Artuso,[21] C. Boulahouache,[21] S. Blusk,[21] J. Butt,[21] E. Dambasuren,[21] O. Dorjkhaidav,[21] J. Haynes,[21] N. Menaa,[21] R. Mountain,[21] H. Muramatsu,[21] R. Nandakumar,[21] R. Redjimi,[21] R. Sia,[21] T. Skwarnicki,[21] S. Stone,[21] J.C. Wang,[21] and Kevin Zhang[21]

(CLEO Collaboration)

[1] *University of Texas - Pan American, Edinburg, Texas 78539*

[2] *Vanderbilt University, Nashville, Tennessee 37235*

[3] *Wayne State University, Detroit, Michigan 48202*

arXiv:hep-ex/0403053v2 30 Mar 2004

[4]*California Institute of Technology, Pasadena, California 91125*

[5]*Carnegie Mellon University, Pittsburgh, Pennsylvania 15213*

[6]*Cornell University, Ithaca, New York 14853*

[7]*University of Florida, Gainesville, Florida 32611*

[8]*University of Illinois, Urbana-Champaign, Illinois 61801*

[9]*Carleton University, Ottawa, Ontario, Canada K1S 5B6*

and the Institute of Particle Physics, Canada

[10]*University of Kansas, Lawrence, Kansas 66045*

[11]*University of Minnesota, Minneapolis, Minnesota 55455*

[12]*Northwestern University, Evanston, Illinois 60208*

[13]*State University of New York at Albany, Albany, New York 12222*

[14]*Ohio State University, Columbus, Ohio 43210*

[15]*University of Oklahoma, Norman, Oklahoma 73019*

[16]*University of Pittsburgh, Pittsburgh, Pennsylvania 15260*

[17]*Purdue University, West Lafayette, Indiana 47907*

[18]*Rensselaer Polytechnic Institute, Troy, New York 12180*

[19]*University of Rochester, Rochester, New York 14627*

[20]*Southern Methodist University, Dallas, Texas 75275*

[21]*Syracuse University, Syracuse, New York 13244*

(Dated: February 7, 2008)

Abstract

We report a new measurement of the B-meson semileptonic decay momentum spectrum that has been made with a sample of 9.4 fb^{-1} of e^+e^- data collected with the CLEO II detector at the $\Upsilon(4S)$ resonance. Electrons from primary semileptonic decays and secondary charm decays were separated by using charge and angular correlations in $\Upsilon(4S)$ events with a high-momentum lepton and an additional electron. We determined the semileptonic branching fraction to be $\mathcal{B}(B \to Xe^+\nu_e) = (10.91 \pm 0.09 \pm 0.24)\%$ from the normalization of the electron-energy spectrum. We also measured the moments of the electron energy spectrum with minimum energies from 0.6 GeV to 1.5 GeV.

PACS numbers: 13.20.He, 12.15.Ff, 14.40.Nd

I. INTRODUCTION

Semileptonic decays of B mesons have been the principal tool for determining the Cabibbo-Kobayashi-Maskawa (CKM) matrix elements V_{cb} and V_{ub} that govern the weak-current couplings of b quarks through external $W^{\pm}$ emission. This reliance results from the inherent simplicity of semileptonic decays, which render more direct access to the underlying quark couplings than do hadronic decays. Nonperturbative hadronic effects play a significant role in the details of semileptonic B decays, however, and pose considerable challenges to the interpretation of precision inclusive and exclusive measurements. This has been demonstrated by puzzles such as a measured B semileptonic branching fraction that has been persistently smaller than theoretical expectations [1, 2, 3, 4, 5].

In recent years, Heavy Quark Effective Theory (HQET) has emerged as a powerful tool in the interpretation of the properties of mesons containing a heavy quark. Rooted in QCD and implemented through the Operator Product Expansion (OPE), HQET provides a rigorous procedure for expressing the observables of semileptonic and rare B decays as expansions in perturbative and non-perturbative parameters [6, 7, 8, 9, 10]. If the validity of this formulation of QCD can be demonstrated by detailed comparison with data, then HQET/OPE can be used to extract the CKM parameter $|V_{cb}|$ from the B semileptonic branching fraction and lifetime with uncertainties that are significantly reduced.

Voloshin first suggested that the moments of the lepton-energy spectrum in inclusively measured semileptonic B decays could provide precise information about the quark-mass difference $m_b - m_c$ [11]. A succession of authors have expanded on this proposal to include moments of other observables of semileptonic decays and the electromagnetic penguin decay $B \to X_s\gamma$ [12, 13]. Measurements have been presented by the CLEO [14, 15] and DELPHI [16] collaborations. Recently, there have been efforts to provide a consistent framework for the interpretation of these measurements. Battaglia *et al.* [17] have performed fits to order $1/m_b^3$ of the preliminary moment measurements of the DELPHI collaboration. Bauer, Ligeti, Luke, and Manohar have presented expressions for various moments of inclusive B decay to order $\alpha_s^2\beta_0$ and Λ_{QCD}^3 for several mass schemes [18]. Fits to the moments of different distributions and to measurements that sample different regions of phase space serve as checks of the overall validity of the HQET/OPE approach. In particular, such tests probe for potential violations of the underlying assumption of quark-hadron duality.

In this paper we present a new measurement of inclusive semileptonic B decays that has been made with the complete data sample obtained with the CLEO II detector at the Cornell Electron Storage Ring (CESR). The momentum spectrum for primary semileptonic decays $B \to Xe\nu$ was isolated through the use of charge and angular correlations in $\Upsilon(4S) \to B\bar{B}$ dilepton events. The technique of using angular correlations in events with a high-momentum lepton was first used by CLEO for measurements of B decays to kaons [19]. It was subsequently applied to measurements of semileptonic B decays by ARGUS [2] and CLEO [3]. In this paper we use the normalization of the measured electron-momentum spectrum to obtain the B semileptonic branching fraction and the detailed shape of the spectrum to measure the electron-energy moments with various minimum-energy cuts. The results presented here supersede the previous CLEO II measurement of the semileptonic branching fraction [3], which was based on the first fifth of the CLEO II data sample. This paper presents an initial interpretation of the electron-energy moments in the context of HQET. A forthcoming publication [20] will provide a comprehensive interpretation of these measurements and other moments of inclusive B decays that have previously been reported by CLEO [14, 21].

II. CLEO II DETECTOR AND EVENT SAMPLE

The CLEO II detector, which has since been replaced by the CLEO III detector, was a general purpose magnetic spectrometer with a 1.5-T superconducting solenoidal magnet and excellent charged-particle tracking and electromagnetic calorimetry. Detailed descriptions of the detector and its performance have been presented previously [22, 23]. Two configurations of the detector were used to collect the data sample of this paper. The first third of the data was obtained with a tracking system that consisted of three concentric cylindrical drift chambers surrounding the beam line. The remaining two thirds were collected after an upgrade that included the replacement of the innermost straw-tube drift chamber with a three-layer silicon vertex detector and a change of the gas mixture from argon-ethane to helium-propane in the main drift chamber. The tracking system provided solid-angle coverage of 95% of 4π in both configurations, and the momentum resolution at 2 GeV/c was 0.6%. The tracking devices also provided specific-ionization measurements for hadron identification, with additional $\pi/K/p$ discrimination provided by a time-of-flight scintillator system

located just beyond the tracking. The final detector system inside the solenoidal magnet was a 7800-crystal CsI (Tl) electromagnetic calorimeter with solid-angle coverage of 98% of 4π. The calorimeter was crucial for electron identification and provided excellent efficiency and energy resolution for photons, yielding a typical mass resolution for π^0 reconstruction of 6 MeV (FWHM). The outermost detector component was the muon identification system, which consisted of layers of proportional-tube chambers embedded at three depths in the iron flux return surrounding the magnet.

The B-meson sample for this analysis was obtained by selecting multihadronic events from 9.4 fb^{-1} of CESR e^+e^- annihilation data at 10.58 GeV, the peak of the $\Upsilon(4S)$ resonance. A requirement of at least five well-reconstructed charged tracks was imposed to suppress low-multiplicity background processes: τ-pair, radiative Bhabha, radiative μ-pair, and two-photon events. Contributions from continuum events $e^+e^- \to q\bar{q}$ (q=d, u, s, or c) were determined with 4.5 fb^{-1} of data collected at a center-of-mass energy approximately 60 MeV below the $\Upsilon(4S)$, where there is no production of $B\bar{B}$. Before subtraction, below-resonance distributions were scaled to account for the difference in the integrated luminosities of the two samples and for the $1/s$ dependence of the $e^+e^- \to q\bar{q}$ cross section. The scale factor was computed with measured integrated luminosities and CESR beam energies, and confirmed by direct determination of the on-resonance/below-resonance ratio of charged-track yields above the kinematic limit for the momenta of B-decay daughters at the $\Upsilon(4S)$. These independent determinations agreed within approximately 0.5%, and a 1% systematic uncertainty in the correction was assumed. The $\Upsilon(4S)$ sample was determined to include 9.7 million $B\bar{B}$ events.

III. SELECTION OF DILEPTON EVENTS

For the measurement of the inclusive electron spectrum in semileptonic B decay, we selected events with a high-momentum (tag) lepton. The tag lepton could be either an electron or a muon, and was required to have a minimum momentum of 1.4 GeV/c and a maximum momentum of 2.6 GeV/c. Such leptons are predominantly produced in the semileptonic decay of one of the two B mesons in an $\Upsilon(4S)$ decay. In events with tags, we searched for an accompanying (signal) electron, with minimum momentum 0.6 GeV/c. These electrons were primarily from the semileptonic decay of the other B meson or from

semileptonic decay of a charmed daughter of either the same or the other B meson. The procedure for disentangling these components is described in Section IV.

All identified leptons were required to project into the central part of the detector ($|\cos\theta| < 0.71$, where θ is the angle between the lepton direction and the beam axis). This fiducial requirement ensured the most reliable and best-understood track reconstruction and lepton identification. Requirements on tracking residuals, impact parameters, and the fraction of tracking layers traversed that had high-quality hits provided additional assurance of reliably determined momenta.

Muons were identified by their ability to penetrate detector material and register hits in the muon chambers. Accepted muon tags were required to reach a depth of at least five nuclear interaction lengths and to have the expected corroborating hits at smaller depths. The efficiency for detecting muons was greater than 90%, and the probability for a hadron track to be misidentified as a muon was less than 1%. Because muons were used only as tags in this analysis, the results are quite insensitive to the details of muon identification.

Electrons were selected with criteria that relied mostly on the ratio of the energy deposited in the electromagnetic calorimeter to the measured momentum (E/p) and on the specific ionization (dE/dx) measured in the tracking chambers. The measurement of the $B \to Xe\nu$ signal spectrum is very sensitive to the details of electron identification; this was the dominant systematic uncertainty in our previous measurement of the $B \to Xe\nu$ spectrum [2]. For this reason, we developed a customized electron-identification procedure for this analysis and have made extensive studies of efficiencies and misidentification rates.

The standard CLEO II electron-identification procedure was a likelihood-based selection that combined measurements of dE/dx, time-of-flight, and calorimeter information including E/p and transverse shower shape. The selection was trained and its efficiency and misidentification probability were determined using data. Electrons from radiative Bhabha events, embedded in hadronic events, were used for the efficiency measurement, and samples of tagged hadron tracks (pions from K^0_S decays, kaons from $D^* \to D^0 \to K^-\pi^+$, and $p/\bar{p}$ from $\Lambda/\bar{\Lambda}$ decays) were used to measure misidentification rates. This procedure provided highly optimized electron identification, with efficiency ranging from 88% at 0.6 GeV/c to 93% at 2.2 GeV/c, as well as hadron-misidentification probabilities that were less than 0.1% over nearly all of the momentum range used for our spectrum measurement.

Detailed studies of the efficiency determination for this standard electron identification

revealed a bias in measurements made with embedded radiative Bhabha events that could be significant for precision measurements. This appeared as a dip in the efficiency beginning at ~ 1.8 GeV/c, which was traced to the inclusion of shower-shape variables in the likelihood. Some electrons from radiative Bhabha events were lost because of distortion of the electron shower due to overlap of the electron and the radiated photon. While radiative Bhabha event-selection cuts were developed to mitigate this effect, it was felt that the associated uncertainty in the momentum dependence of the electron-identification procedure would be a significant systematic limitation on our spectrum measurement. Since the background due to misidentified hadrons was judged to be negligible at higher momenta, we developed an alternative procedure that sacrificed some background rejection in favor of a more reliably determined efficiency. The new procedure used the full likelihood analysis below 1 GeV/c and simple cuts on the key variables above 1 GeV/c: E/p between 0.85 and 1.1 and measured dE/dx no more than 2σ below the expected value for an electron. A time-of-flight requirement provided additional hadron (primarily kaon) rejection between 1.0 and 1.6 GeV/c. There was no requirement on shower shape above 1 GeV/c, and the previously mentioned momentum-dependent bias was eliminated.

We used several "veto" cuts to minimize backgrounds from sources other than semileptonic decays. We eliminated any tag or signal electron that could be paired with another lepton of the same type and opposite charge if the pair mass was within 3σ of the J/ψ mass. Monte Carlo simulations showed this veto to be approximately 58% efficient in rejecting electrons from J/ψ, while introducing an inefficiency of 0.5% into the selection of electrons from semileptonic B decays. Electrons from π^0 Dalitz decays were rejected when the three-body invariant mass of a combination of the candidate electron, any oppositely charged track of momentum greater than 0.5 GeV/c and a photon was within 3σ of the π^0 mass. In this case, the efficiency for rejection was 29% and the inefficiency for semileptonic-decay electrons was less than 0.5%. Photon conversions were rejected based on track-quality variables (e.g. the distance of closest approach to the event vertex) and on the properties and locations of vertices formed by pairing electron candidates with oppositely charged tracks. These criteria were found to be 56% efficient in rejecting electrons from photon conversions and to contribute an inefficiency for detecting electrons from $B \to Xe\nu$ of 2%. For each of these vetoed processes, Monte Carlo simulations were used to estimate the background that "leaked" into our final sample, as is discussed in Sec. V.

	Unmixed Events	**Mixed Events**
Primary Events	$\ell^+ \leftarrow \bar{b} \qquad b \longrightarrow e^-$	$\ell^+ \leftarrow \bar{b} \qquad \bar{b} \longrightarrow e^+$
Opposite B Secondary Events	$\ell^+ \leftarrow \bar{b} \qquad b \rightarrow c \rightarrow e^+$	$\ell^+ \leftarrow \bar{b} \qquad \bar{b} \rightarrow \bar{c} \rightarrow e^-$
Same B Secondary Events	$\ell^+ \leftarrow \bar{b} \longrightarrow \bar{c} \rightarrow e^-$	

TABLE I: Charge correlations for dilepton $B\bar{B}$ events. The ℓ^+ denotes the tag lepton.

IV. MEASUREMENT OF THE ELECTRON MOMENTUM SPECTRA IN LEPTON-TAGGED EVENTS

A. Method

The determination of the B-meson semileptonic branching fraction and electron-energy moments demands a background-free sample of $B \rightarrow X\ell\nu$ decays that covers as much of the available phase space as possible. The requirement of a lepton tag of minimum momentum 1.4 GeV/c in $\Upsilon(4S) \rightarrow B\bar{B}$ events selects a sample of semileptonic B decays that is more than 97% pure. This allows study of "signal" electron production from the other B in the event with small backgrounds and components that can be readily disentangled by using charge and kinematic correlations. In our analysis we searched for signal electrons with momenta of at least 0.6 GeV/c. This minimum-momentum requirement was a compromise, allowing measurement of approximately 94% of the full B semileptonic decay spectrum, while excluding low-momentum electrons for which the systematic uncertainties in efficiency determinations and hadronic backgrounds were significant.

There are three main sources of signal electrons in lepton-tagged events, summarized in Table I. The key to discriminating among these sources is to measure the spectra of signal electrons separately for events with a tag of the same charge and for those with a tag of the opposite charge. Semileptonic decay of the other B meson gives a signal electron with charge opposite to that of the tag (if $B^0\bar{B}^0$ mixing is ignored). Semileptonic decay of a charm meson that is a daughter of the other B gives a signal electron of the same charge as the tag (again ignoring $B^0\bar{B}^0$ mixing). Semileptonic decay of a charm meson from the same B gives a signal electron with the opposite charge from the tag, but with a kinematic signature that makes its contribution easy to isolate. The effect of $B^0\bar{B}^0$ mixing is to reverse

the charge correlations in a known proportion of events. We use these charge correlations to extract statistically the primary and secondary spectra from the unlike-sign and like-sign spectra. We assume that charged and neutral B mesons have the same decay rates and lepton-energy spectra for primary semileptonic decays.

Discrimination of same-B signal electrons from opposite-B signal electrons in the unlike-sign sample relies on the kinematics of production just above $B\bar{B}$ threshold. At the $\Upsilon(4S)$, the B and the $\bar{B}$ are produced nearly at rest. There is little correlation between the directions of a tag lepton and of an accompanying electron if they are the daughters of different B mesons. If they originate from the same B, however, there is a strong tendency for the tag and the electron to be back-to-back. The correlation between the opening angle $\theta_{\ell e}$ of the tag lepton and the signal electron and the signal electron momentum p_e has been studied with Monte Carlo simulations of $B\bar{B}$ events and is illustrated in Fig. 1. For unlike-sign

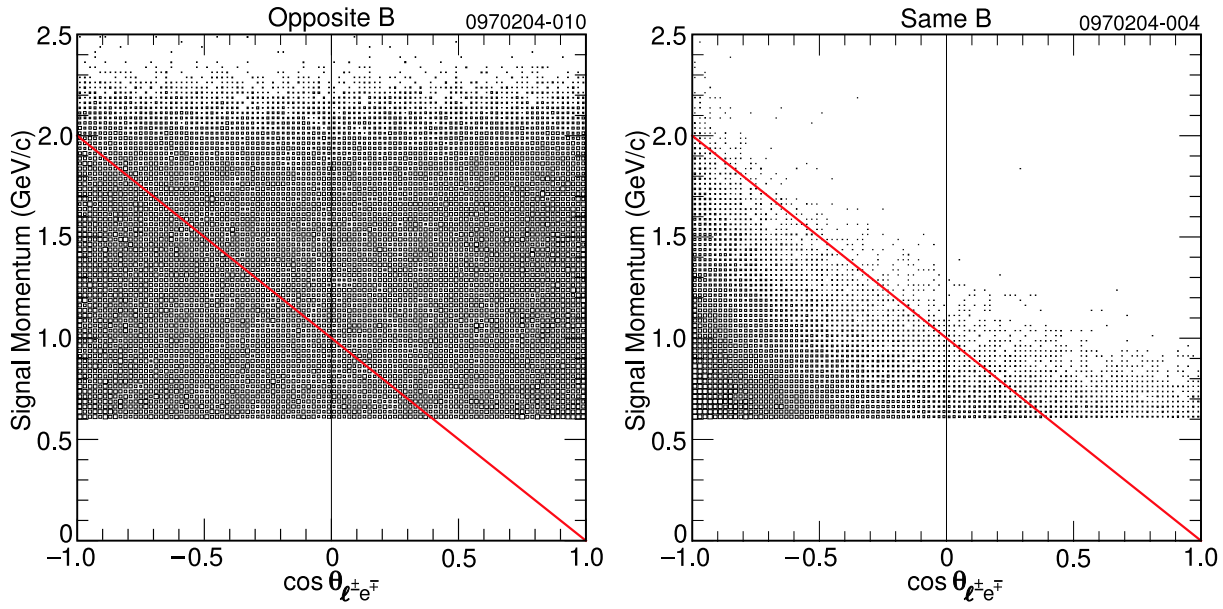

FIG. 1: Monte Carlo simulation of electron momentum versus the cosine of the opening angle between the tag lepton and the signal electron (cos θ_{le}) for unlike-sign dilepton pairs from opposite B's (top) and from the same B (right). The line indicates $p_e + \cos\theta_{le} = 1$.

pairs we applied the "diagonal cut" $p_e + \cos\theta_{\ell e} \geq 1$ (p_e in GeV/c). This cut suppressed the same-B background by a factor of 25, while retaining two-thirds of the opposite-B unlike-sign electron signal. The residual contribution of same-B secondaries that leak through the diagonal cut is small and is estimated with Monte Carlo normalized to the data as described in Sec. IV B. We performed extensive Monte Carlo studies of potential bias that might have

been introduced into our analysis by this cut. Semileptonic decays $B \to X_c \ell\nu$ in $B\bar{B}$ events were simulated as a mixture of resonant and nonresonant decays. These used HQET and the CLEO-measured form-factor parameters for $B \to D\ell\nu$ [24] and $B \to D^*\ell\nu$ [25], and models for $B \to D^{**}\ell\nu$ [26] and nonresonant modes $B \to DX\ell\nu$ [27]. These studies demonstrated that the efficiency was essentially independent of the B-decay mode. Different backgrounds were affected quite differently by this cut, however, and these effects were included in the associated systematic uncertainties. This is discussed in Sec. V.

Because the diagonal cut largely eliminated the same-B background from the unlike-charge sample, the electron spectra for events with unlike-sign tags ($\frac{dN(\ell^\pm e^\mp)}{dp}$) and for events with like-sign tags ($\frac{dN(\ell^\pm e^\pm)}{dp}$) included only primary B semileptonic decays and secondary charm semileptonic decays from events in which the tag lepton and the signal electron were daughters of different B mesons. Assuming universality of the secondary-charm lepton spectra (we discuss the validity of this assumption below), Eqs. (1) and (2) provide the connection between these measured spectra and the differential branching fractions for primary ($\frac{d\mathcal{B}(b)}{dp}$) and secondary ($\frac{d\mathcal{B}(c)}{dp}$) decays.

$$\frac{dN(\ell^\pm e^\mp)}{dp} = N_\ell\, \eta(p)\, \epsilon(p) \left[\frac{d\mathcal{B}(b)}{dp}\,(1-\chi) \;+\; \frac{d\mathcal{B}(c)^{oppB}}{dp}\,\chi \right] \tag{1}$$

$$\frac{dN(\ell^\pm e^\pm)}{dp} = N_\ell\, \eta(p) \left[\frac{d\mathcal{B}(b)}{dp}\,\chi + \frac{d\mathcal{B}(c)^{oppB}}{dp}\,(1-\chi) \right] \tag{2}$$

In these equations, N_ℓ is the effective number of tags in the sample, p is the signal electron momentum, $\eta(p)$ is the efficiency for reconstructing and identifying the electron, $\epsilon(p)$ is the efficiency of the diagonal cut applied to the unlike-sign sample, and χ is the $B^0\bar{B}^0$ mixing parameter multiplied by the fraction of all $B\bar{B}$ events at the $\Upsilon(4S)$ that are neutral B's.

We determined χ by combining several pieces of experimental information. The Particle Data Group value for the $B^0_d\overline{B^0_d}$ mixing parameter is $\chi_d = 0.181 \pm 0.004$ [28]. The charged/neutral B lifetime ratio is $\tau^\pm/\tau^0 = 1.083 \pm 0.017$ [28]. CLEO has measured the ratio of charged to neutral B production at the $\Upsilon(4S)$ to be $\frac{f_{+-}\tau_\pm}{f_{00}\tau_0} = 1.11 \pm 0.08$ [29]. From these inputs we found $\chi = f_{00}\chi_d = 0.089 \pm 0.004$, which has been used in extracting the primary and secondary spectra.

Eqs. (1) and (2) were derived under the assumption that the secondary-charm lepton spectra are the same for charged and neutral B events. This assumption was made for our

previous lepton-tagged measurement of $B \to X\ell\nu$ [3, 30] and is inconsistent with currently available data.

Modifying Eqs. (1) and (2) to allow for the different secondary spectra in charged and neutral events, and solving the resulting equations for the primary and secondary spectra leads to Eqs. (3) and (4).

$$\frac{d\mathcal{B}(b)}{dp} = \frac{1}{(1-[\Delta(p)+1]\,\chi)}\frac{1}{N_\ell\,\eta(p)}\left[\frac{[1-\chi\Delta(p)]}{\epsilon(p)}\frac{dN(\ell^\pm e^\mp)}{dp} - \chi\Delta(p)\frac{dN(\ell^\pm e^\pm)}{dp}\right] \quad (3)$$

$$\frac{d\mathcal{B}(c)}{dp} = \frac{1}{(1-[\Delta(p)+1]\,\chi)}\frac{1}{N_\ell\,\eta(p)}\left[\frac{\chi}{\epsilon(p)}\frac{dN(\ell^\pm e^\mp)}{dp} - (1-\chi)\frac{dN(\ell^\pm e^\pm)}{dp}\right] \quad (4)$$

The new factor $\Delta(p)$ accounts for the secondary-spectra differences in charged and neutral events. We determined $\Delta(p)$ with Monte Carlo simulations incorporating all relevant information on charm and B production and decay at the $\Upsilon(4S)$ as compiled by the Particle Data Group [28]. Specifically, $\Delta(p)$ reflects the combined effect of the different branching fractions for $B^0 \to \bar{D}^0 X$, $B^0 \to D^- X$, $B^+ \to \bar{D}^0 X$, and $B^+ \to D^- X$, the difference between the semileptonic branching fractions of charged and neutral D's, and $B^0\bar{B}^0$ mixing. Fig. 2 shows the $\Delta(p)$ obtained in our study. The systematic uncertainty introduced by this correction was assessed as half of the difference between results obtained with $\Delta(p)$ as shown in Fig. 2 and those obtained with $\Delta(p) = 1$, which recovers the previous assumption. More detail on this correction can be found in Ref. [31].

In the following three sections we describe the determination of the charge-separated spectra, their backgrounds, the efficiencies, and the final extraction of the primary spectrum. The systematic uncertainties that affect all quantities derived from the measured primary spectrum are discussed in Sec. V.

B. Charge-Separated Spectra and Background Corrections

The raw $\Upsilon(4S)$ electron momentum spectra for the unlike-sign sample with the diagonal cut applied and for the like-sign sample are shown in Fig. 3. These raw spectra include several backgrounds that had to be subtracted before the $B \to Xe\nu$ spectrum could be obtained. Some of this background was due to real electrons that entered the sample because of false muon or electron tags. The false tags included hadrons misidentified as leptons ("fakes")

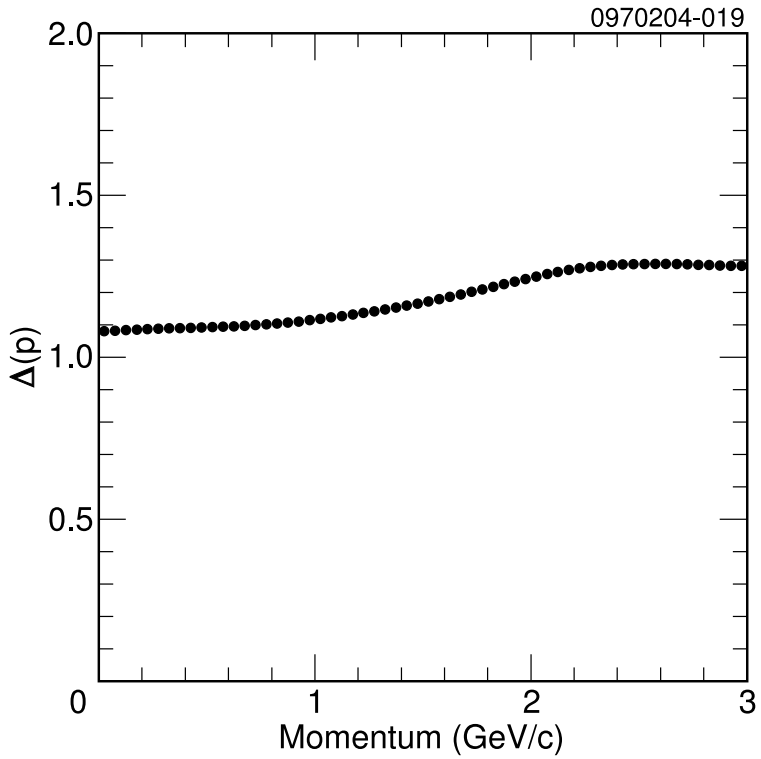

FIG. 2: Secondary correction factor $\Delta(p)$.

and real leptons from processes other than semileptonic B decays. Among the latter were leptons from semileptonic decays of charmed particles, leptons from J/ψ decays, π^0 Dalitz decays and photon conversions that leaked through one of the vetoes, and leptons from other sources in B decays, including leptonic decays of τ, leptonic decays of ψ' and Dalitz decays of η. The minimum momentum requirement for tag selection of 1.4 GeV/c ensured that these backgrounds were small.

Background processes contributing directly to the signal electrons for events with true lepton tags were somewhat larger. These included fakes, the sources of real leptons listed above as contributing to the tags, and several other mechanisms yielding real electrons. Most charmed-meson semileptonic decays were not treated as background, but were isolated algebraically using Eqs. (3) and (4) as described in Sec. IV D. Three sources of electrons from charm were subtracted as backgrounds. The first was the small component of unlike-sign electrons from same-B charm decays that passed the diagonal cut. The second was electrons from decays of "upper-vertex" charm daughters of the other B ($b \to cW^+$, $W^+ \to c\bar{s}$), which was an unlike-sign contribution that could not be distinguished kinematically from

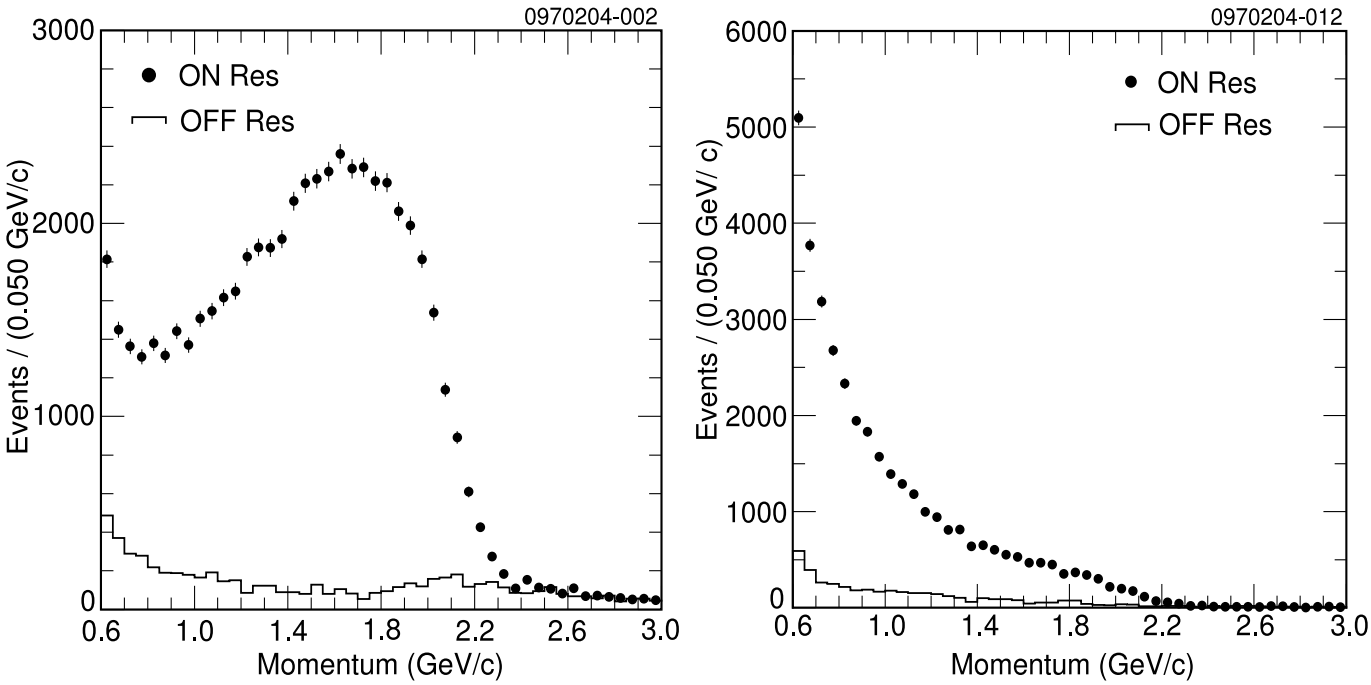

FIG. 3: Electron-momentum spectra for (left) unlike-sign pairs passing the diagonal cut, and (right) like-sign pairs without the cut. The points represent data collected on the $\Upsilon(4S)$ peak and the histograms are the estimated continuum contributions determined with scaled below-resonance data.

the $B \to Xe\nu$ signal. The third was electrons from the decay of charmed-baryons.

The background due to both tag and signal fakes in the $B\bar{B}$ spectra was estimated by combining misidentification probabilities per track, binned in momentum, with the hadronic track momentum spectra obtained from data by imposing all selection criteria except for lepton identification. These track spectra were corrected for the contributions of real leptons. The misidentification probabilities were measured with samples of pions from reconstructed K^0_S decays, kaons from $D^* \to D \to K\pi$ and protons and antiprotons from the decays of Λ and $\bar{\Lambda}$. Monte Carlo simulations were used to correct the measured muon misidentification probabilities for the small underestimate that resulted when pion or kaon decays in flight prevented the successful reconstruction of the K^0_S or D, but not the misidentification as a muon. Relative particle abundances as a function of momentum were determined with Monte Carlo and used to combine the measured pion, kaon and $p/\bar{p}$ fake rates into misidentification probabilities per hadron track that were appropriate for B decays.

The backgrounds due to veto leakage in the tag and signal samples were estimated by

Monte Carlo simulation. The normalization for this correction was determined from data by fitting the spectra of vetoed leptons in Monte Carlo to the corresponding spectra in the data. The fits demonstrated that the Monte Carlo does a very good job of reproducing the observed distributions, in particular for J/ψ, which is the most important veto.

The leakage of same-B secondary signal electrons was estimated with a procedure similar to that for the veto leakage. In this case, the two-dimensional distribution of $\cos\theta_{\ell e}$ versus signal-electron momentum was fitted. Again, the normalization was determined by fitting the Monte Carlo distributions for same-B secondary signal electrons that failed the diagonal cut to the corresponding distribution in data. This factor was then used to scale the Monte Carlo distributions for those that leaked through the cut, providing the background correction that was applied to the electron spectrum.

Other physics backgrounds to both tags and signals were estimated with Monte Carlo simulations, primarily a sample of "generic" $B\bar{B}$ events with neutral B mixing modeled to agree with present experimental observations. This simulated sample had five times the statistics of $\Upsilon(4S)$ data sample.

Fig. 4 shows the continuum-subtracted unlike-sign and like-sign spectra together with

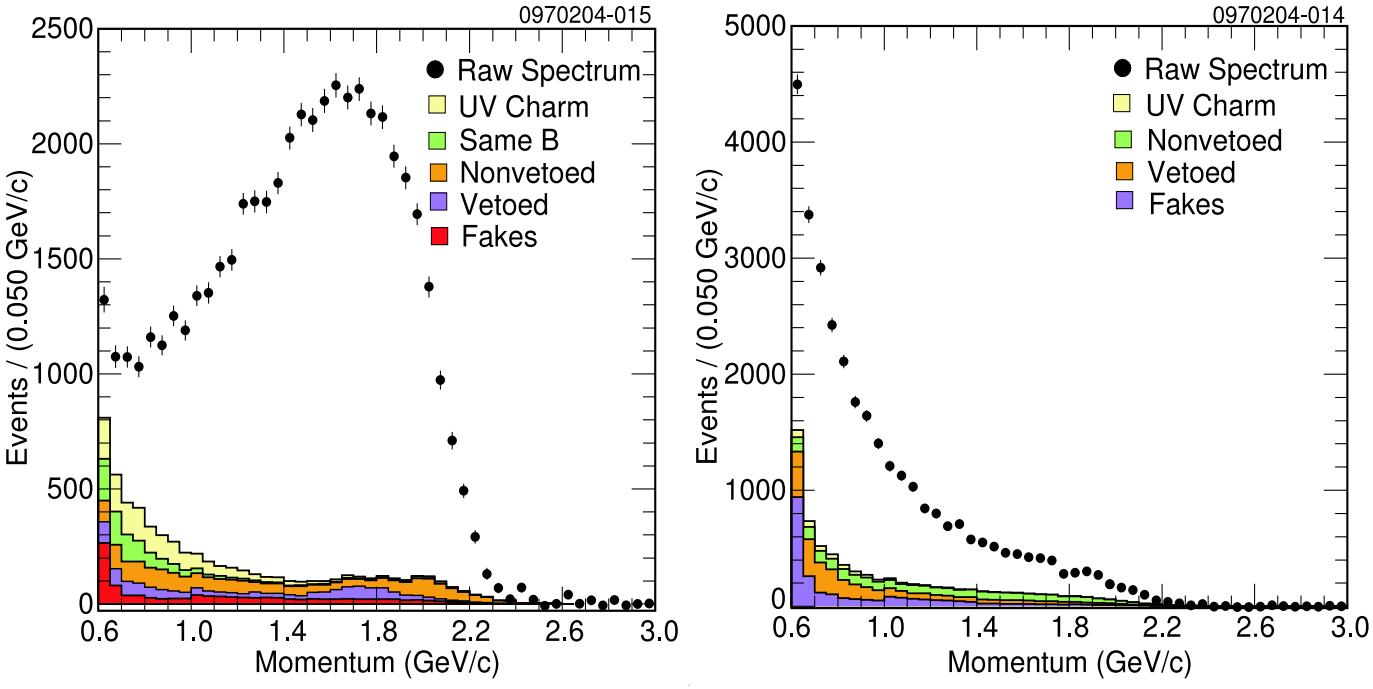

FIG. 4: Continuum-subtracted unlike-sign (left) and like-sign (right) spectra, showing the breakdown of backgrounds computed as described in the text.

the backgrounds determined with the procedures described above. Sources of both tag-lepton and signal-electron backgrounds have been combined in these plots. For example, electrons that are the direct product of an upper-vertex charm decay and electrons that are accompanied by a tag from an upper-vertex charm decay are both included in the category "UV charm." The spectra after the subtraction of all backgrounds are shown in Fig. 5. Systematic uncertainties in the background corrections are described in Sec. V.

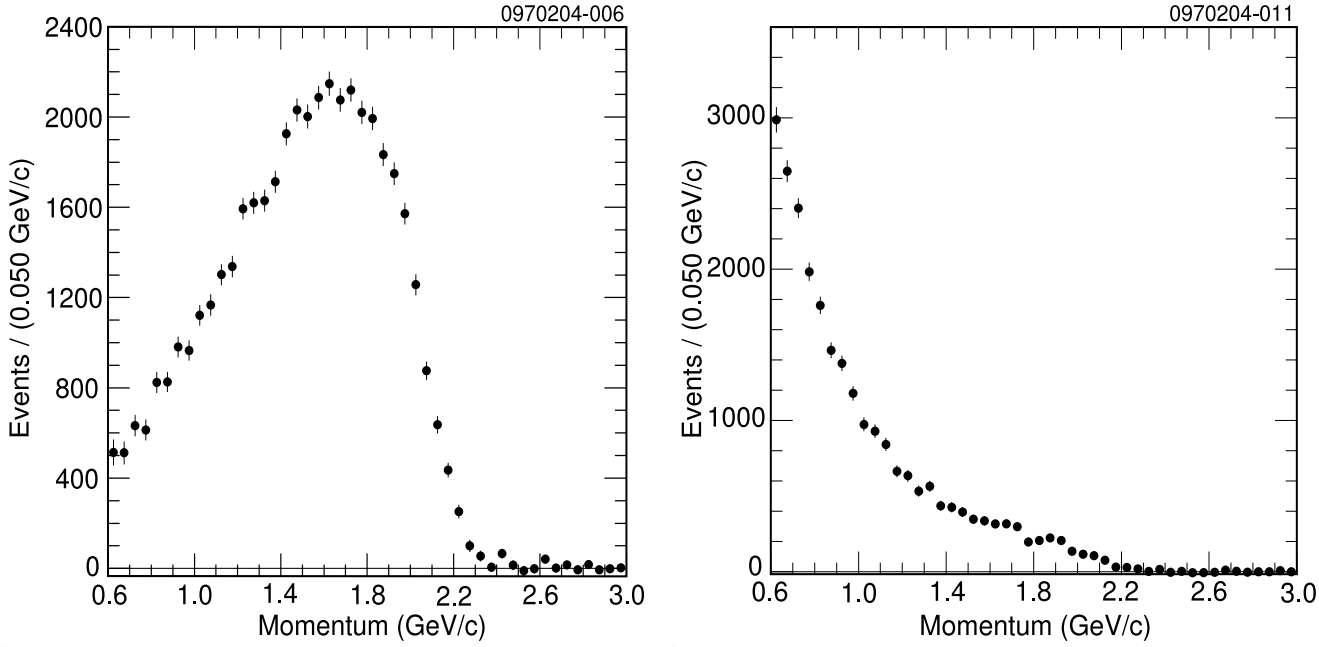

FIG. 5: Unlike-sign (left) and like-sign (right) electron spectra after all backgrounds have been subtracted. These are the spectra that were passed to Eqs. (3) and (4).

C. Counting Tags

The normalization for the measurement of the B semileptonic branching fraction is provided by N_ℓ, the effective number of tags in our lepton-tagged event sample. Its determination is given in Table II. Identified leptons satisfying the tag requirements of Sec. III were counted for both the on-$\Upsilon(4S)$ and below-resonance data samples. After correction for the continuum, fake leptons, and other backgrounds by the procedures described in Sec. IV B, the raw number of tags from semileptonic B decays was found to be $N_\ell^{\rm raw} = 1,137,042 \pm 1631$, where the error is statistical only.

It was not necessary to correct the tag count for the absolute efficiencies of lepton selec-

Source	μ	e	$\mu + e$
ON $\Upsilon(4S)$	828,155 ± 910	837,002 ± 915	1,665,157 ± 1,290
Scaled Continuum	261,667 ± 737	212,146 ± 664	473,813 ± 992
Cont. Subtracted	566,488 ± 1,171	624,856 ± 1,131	1,191,344 ± 1,628
Fake Leptons	11,385 ± 61	936 ± 4	12,321 ± 61
J/ψ	3,397 ± 28	4,451 ± 31	7,848 ± 42
π^0	N/A	190 ± 8	190 ± 8
γ	N/A	116 ± 6	116 ± 6
Secondary Charm	10,484 ± 47	13,347 ± 52	23,831 ± 70
Upper-Vertex D	330 ± 9	417 ± 9	747 ± 13
Upper-Vertex D_s	2,364 ± 22	818 ± 13	3,182 ± 26
τ	1,947 ± 20	2,538 ± 22	4,485 ± 30
ψ'	588 ± 11	609 ± 11	1,197 ± 16
Other Backgrounds	356 ± 9	29 ± 3	385 ± 9
Background-Subtracted Yield	535,637 ± 1,174	601,405 ± 1,132	1,137,042 ± 1,631

TABLE II: Yields and backgrounds for tag count. Errors are statistical only.

tion, such as track-quality requirements and lepton identification, because the background-corrected sample of events with tags provides us with $B\bar{B}$ events in which one B is known to have decayed semileptonically. It is the fraction of these events in which the other B decayed to an electron that gives the semileptonic branching fraction. The only necessary corrections to the tag count are for effects that result preferentially in the gain or loss of events in which both B's decayed semileptonically.

Such a correction to the tag count was necessitated by the effect of the charged multiplicity requirement in the event selection, since semileptonic decays typically have lower multiplicity than hadronic decays. We evaluated this effect with a large sample of simulated $B\bar{B}$ events. The event-selection efficiency ϵ_ℓ for any event with a lepton tag from semileptonic B decay was found to be 95.8%, while the efficiency $\epsilon_{\ell e}$ for events with a lepton tag and a second semileptonic B decay was 91.0%. This gives a relative event-selection efficiency of $\epsilon_r = \epsilon_{\ell e}/\epsilon_\ell = 95.0\%$, showing that our direct tag count was an overestimate of the true number

of events with tags that could enter our primary spectrum. Therefore, the effective number of tags was $N_\ell = \epsilon_r N_\ell^{\rm raw} = 1,079,901 \pm 1,549$ (statistical uncertainty only).

This relative event-selection efficiency introduced a systematic uncertainty into our measurement associated with how well the Monte Carlo simulated the multiplicity of both hadronic and semileptonic B decays. We compared the observed charged multiplicity distributions for $B\bar{B}$ events in data and in Monte Carlo and found the agreement to be quite good. The measured mean multiplicities agreed within 0.1 unit for all events with tags, and within 0.01 unit for events with tags and electrons from $B \to Xe\nu$. The latter difference was determined to be negligible, and the systematic uncertainty associated with the former was assessed by reweighting the Monte Carlo sample in event multiplicity.

We note here that there was a misconception in the treatment of this effect in our previous analysis [3], which is superseded by this paper. In that case, the relative event-selection efficiency was calculated with a numerator that included all signal electrons, not just the primary $B \to Xe\nu$ electrons. Including all dilepton events in the numerator had the effect of raising the average charged multiplicity in those events, since it admitted cases where an electron is produced further down the decay chain, with more accompanying hadrons. When calculated in this incorrect way, the relative event-selection efficiency was overestimated and the semileptonic branching fraction underestimated by a few percent relative.

D. Efficiencies and Extracted Primary and Secondary Spectra

To extract the primary and secondary spectra, the remaining step was the substitution of our corrected yields into Eqs. (3) and (4). In addition to the quantities already given, this required determination of the efficiencies $\eta(p)$ and $\epsilon(p)$ for the detection of the electron and the effect of the diagonal cut on the opposite-sign sample, respectively. The electron detection efficiency $\eta(p)$ includes the efficiency of the fiducial cut on electron candidates, the efficiency of track-quality cuts, the efficiency of the electron identification, and the efficiency for passing the three vetoes (J/ψ, π^0 Dalitz, γ-conversion). Each of these, except for the electron identification, was obtained by processing Monte Carlo simulations of $\Upsilon(4S)$ events. Where possible, the Monte Carlo was normalized or validated with data. The bin-by-bin effect of bremsstrahlung in the detector material was also incorporated into the efficiency through this simulation.

Studies of electron-identification and track-selection efficiencies were performed with tracks from radiative Bhabha events embedded into hadronic events. The "target" hadronic events were selected to ensure that the final embedded samples were compatible with $B\bar{B}$ signal events in event topology, multiplicity and electron angular distribution. For the tracking studies, embedded samples were prepared for both data and Monte Carlo, and comparison of the two gave a correction factor as a function of electron momentum that could subsequently be applied to the efficiency determined with simulated signal events. For the track-selection criteria used in this analysis, the correction factor proved to be almost negligibly different from unity.

The embedded radiative Bhabha sample was also used to measure the efficiency of our electron-identification package. In this case the efficiency determined for electrons in the embedded sample was applied directly to data, and extensive studies were made of systematic uncertainties. These studies are described in Sec. V.

With all ingredients assembled, the final step was substitution into Eqs. (3) and (4) to obtain the separated primary and secondary spectra. These are shown in Fig. 6. The apparent pairing of points on the rising side of the primary spectrum has been studied extensively. It is not attributable to any one step of the analysis procedure, and we have found no other explanation other than a statistical fluctuation. Sec. VI and Sec. VII describe

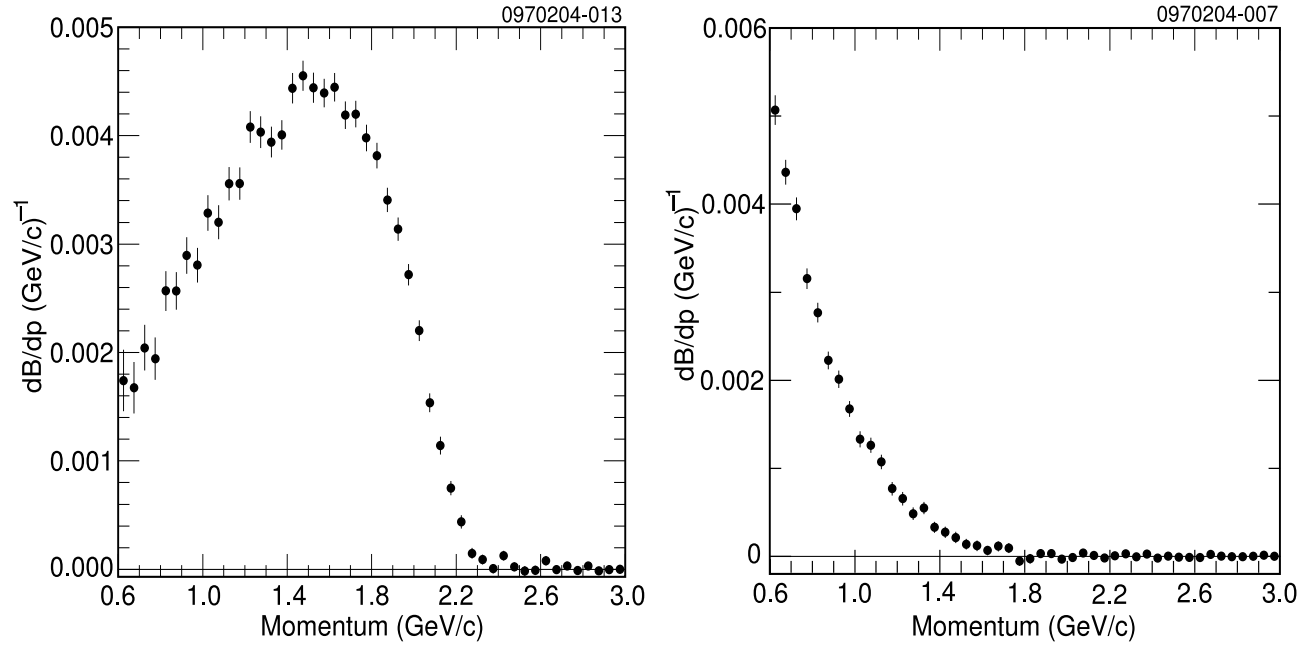

FIG. 6: Primary (left) and secondary (right) spectra, obtained by solving Eqs. (3) and (4).

the extraction of the $B \to Xe\nu$ branching ratio and the electron-energy moments from the primary spectrum, respectively. Sec. V provides details on the systematic uncertainties of the spectrum measurement that are common to both.

V. SYSTEMATIC UNCERTAINTIES AND CROSS-CHECKS

Nearly all of the systematic uncertainties in the measurements of the B semileptonic branching fraction and the electron-energy moments are rooted in the systematic uncertainties in the spectrum measurement. Many of these have already been identified, and this section provides additional details about their evaluation. The actual systematic uncertainty estimates are presented in Sec. VI and Sec. VII. Full details of the systematic studies are available in Ref. [31].

A. Veto-Leakage Corrections

These corrections were computed using momentum spectra determined from Monte Carlo simulations with normalizations obtained by fitting data, as described in Sec. IV B. This procedure ensured that the corrections were insensitive to uncertainty in the rates of the contributing processes, although there remained some sensitivity to the modeling of details like the momentum spectra. The J/ψ modeling is believed to be very accurate: the mixture of decays was tuned to agree with exclusive branching ratios [28] and the inclusive J/ψ momentum spectrum [32]. We estimated a $\pm 5\%$ systematic uncertainty on the subtraction of unvetoed J/ψ's. For the π^0 and photon-conversion vetoes, there was more uncertainty in the simulation of the detector response, and we took $\pm 20\%$. For each of these, we have fluctuated the correction upward and downward by these amounts and taken the systematic uncertainty on any observable to be one-half of the difference between them.

B. Same-B Secondaries

The background due to same-B secondaries that were not eliminated by the diagonal cut was also computed with Monte Carlo normalized to data, as described in Sec. IV B. In this case, the yield and distribution for the same-B secondaries that were successfully cut (98%)

were used to normalize the distribution for those that leaked through (2%), with negligible statistical uncertainty. An excellent fit was obtained in the two dimensions of opening angle versus momentum, demonstrating that the Monte Carlo did a very good job of reproducing the detailed distributions of the contributing processes. The systematic uncertainty for this correction was taken to be 15%.

C. Other Non-Vetoed Background Corrections

Similar to the method of determining the systematic errors attached to veto leakage, we used the Monte Carlo to simulate the shapes of the momentum spectra for backgrounds due to non-vetoed physics processes. For each component we attempted to assess a reasonable uncertainty based on world-average branching fractions and other information. In all cases we take as the systematic uncertainty one-half of the difference between the extreme variations.

Upper-vertex charm was the largest of these sources. Broadly speaking, this background can be broken down into two components: final states with a D_s meson and another charmed particle and final states with two non-strange charmed mesons. We treated these independently, since their estimates are largely based on different experimental and theoretical inputs. While the semileptonic branching fraction $\mathcal{B}(D_s \to Xe\nu)$ is not well measured, the D^0 and D^+ semileptonic branching fractions can be combined with lifetime data to estimate $\mathcal{B}(D_s \to Xe\nu) \simeq 8\%$, an estimate that is probably reliable at the 10% level. However, this uncertainty is essentially negligible compared to that in the branching fraction for $B \to D_s X$, which has been estimated to be $9.8 \pm 3.7\%$ [33], based on a variety of exclusive measurements. Using these assumptions, we took the overall systematic uncertainty on the contribution of semileptonic decays of upper-vertex D_s to be $\pm 40\%$.

The upper-vertex D contribution is somewhat better known, with well-measured semileptonic branching fractions [28] and an estimated rate for $B \to \bar{D} D^{(*)} X$ of $8.2 \pm 1.3\%$ [33]. We assigned a systematic uncertainty to the electrons from upper-vertex non-strange charmed mesons of $\pm 25\%$.

The estimated contributions of $B \to \tau \to e$ and $B \to \psi' \to e^+e^-$ were both based on world-average measured branching fractions [28]. Both were assigned systematic errors of $\pm 15\%$, taking into account the errors of those branching fractions, with some additional

uncertainty associated with the shapes of the momentum spectra.

D. Lepton Identification

Since muons were only used for tags, the correction for fake muons only entered our results through the normalization of the primary spectrum. We took an overall systematic uncertainty in the estimate of muon fakes of ±25%. The muon-identification efficiency was not used in our measurement.

For our previous lepton-tagged analysis [3], the results obtained were yields and branching fractions with sensitivity only to the momentum-averaged efficiency. It was therefore unnecessary to scrutinize carefully the reliability of the measured momentum dependence of the electron-identification efficiency. The determination of the spectral moments of the electron energy spectrum was much more demanding in this regard. As has been described in Sec. III, momentum-dependent biases in the radiative-Bhabha-measured efficiency for the standard CLEO II electron-identification package led us to reoptimize with simpler criteria.

Two approaches were used to assess the systematic uncertainties in electron identification. In the first, estimates were made based on studies of the radiative Bhabha and tagged-track samples that were used to determine the efficiency and misidentification probabilities. These involved techniques like varying selection cuts and comparison of embedded and unembedded samples that clearly probed systematic effects, but were difficult to use for a quantitative assessment. Overall uncertainties were estimated to be in the range of 2% for the electron-identification efficiency. For the misidentification probability the uncertainty was estimated to increase from 25% below 1 GeV/c to 100% above 1.5 GeV/c. Uncertainty in the momentum dependence was very difficult to assess. Monte Carlo studies were inconclusive, and the effect on the electron-identification efficiency was bracketed by "worst-case skewing" of the radiative Bhabha measurement.

This approach was deemed to be unsatisfactory for the moments measurement, so we developed a second procedure that relied on the "factorizability" of our simplified electron identification. Each of the component criteria of the electron identification (dE/dx requirement, low-side E/p cut, high-side E/p cut, time-of-flight, likelihood cut for momenta below 1 GeV/c), was separately adjusted and the entire analysis, including efficiency and fake-rate determinations, was repeated. The amount of "knob-turning" was determined based on the

inefficiency associated with each cut, which was typically a few per cent. The target was a tightening of the cut sufficient to double its inefficiency. In the cases of the less powerful elements of the selection (dE/dx and time-of-flight), the alternative was to turn off that cut completely. The resulting primary spectra were processed to obtain the observables of our analysis, the branching fraction and moments, and the difference between the results for the standard and modified analyses was taken as the systematic uncertainty associated with that component of the electron identification. Since the five different knobs represented independent elements of the electron selection, we combined their systematic uncertainties in quadrature.

E. Other Efficiency Corrections

The track-selection efficiency was determined with a Monte Carlo simulation of signal events, corrected by the data/Monte Carlo ratio determined with embedded radiative Bhabha events, as described in Sec. IV D. The systematic error associated with this efficiency was assigned to be the difference between results obtained with the standard spectrum, and those obtained without application of the data/Monte Carlo correction.

We set the systematic uncertainty due to the efficiency of the diagonal cut based on extreme variations of the mixture of semileptonic B decays in our simulated event sample. Variations were constrained by measured branching fractions [28]. The mixtures considered ranged from the "hardest possible" primary spectrum ($B \to D^* e\nu$ increased by 6%; $B \to D^{**} e\nu$ increased by 30%; $B \to De\nu$ decreased by 8%; nonresonant $B \to D^{(*)} X e\nu$ decreased by 30%) to the "softest possible" primary spectrum (reverse of the above variations). For each case we computed a new diagonal cut efficiency, rederived the final spectrum, and calculated new values for the observables. Half the difference between the two extremes was used as the systematic uncertainty associated with the diagonal cut efficiency.

We calculated the systematic error due to the efficiency correction of the $J/\psi, \pi^0$, and γ-conversion vetoes by using the "hardest" and "softest" primary-spectrum variations, as in the determination of the diagonal cut systematic. We then took as the error half the difference between the "hardest" and "softest" variations, plus 10% of itself. This extra 10% on the error was to account for the fact that we only varied about 90% of the primary spectrum when we reweighted the unlike-sign spectrum. Because of mixing, the other 10%

of the primary electrons appeared in the like-sign spectrum.

F. $\Delta(p)$ and $B^0\overline{B^0}$ Mixing

The factor $\Delta(p)$ accounts for the difference between the secondary-electron spectra in charged and neutral B decays, as described in Sec. IV A. The systematic uncertainty assigned to this was taken to be half of the difference between results obtained from Eqs. (3) and (4) with the $\Delta(p)$ determined in our Monte Carlo study (standard case) and those obtained by taking with $\Delta(p) = 1$ (no correction).

The uncertainty on the mixing parameter χ was determined from relevant input data, as is described in Sec. IV A. The effect on measured quantites was determined by solving for the spectra with values of χ that were shifted up and down by 1σ.

G. Cross-Checks

We also performed several cross-checks of our results to test all aspects of the analysis procedure and to verify that there were no biases in the determination of the B semileptonic branching fraction and electron-energy moments. A $B\bar{B}$ Monte Carlo sample with known semileptonic branching fraction and spectral shape was subjected to nearly the full analysis procedure. Results obtained were consistent with inputs and generator-level quantities to within statistical errors.

Other cross-checks involved subdividing the data sample in various ways to demonstrate that there were no unexpected dependences in the results. No statistically significant differences were found between the subsample with electron tags and that with muon tags, between positively charged and negatively charged tags, between low-momentum (< 1.75 GeV/c) and high-momentum (> 1.75 GeV/c) tags, or between the data samples collected before and after the detector upgrade. More details on these cross-checks can be found in Ref. [31].

VI. B SEMILEPTONIC BRANCHING FRACTION

Integrating the measured primary spectrum in Fig. 6 between 0.6 GeV/c and 2.6 GeV/c gives the partial branching fraction $\mathcal{B}(B \to Xe\nu, p > 0.6 \text{ GeV}/c) = (10.21 \pm 0.08 \pm 0.22)\%$, where the first uncertainty is statistical and the second is the systematic uncertainty associated with measurement of the electron spectrum (Sec. V). This result is almost completely free of model dependence. To extract the full semileptonic branching fraction, it is necessary to correct for the undetected portion of the electron spectrum below the low-momentum limit of 0.6 GeV/c.

To determine this fraction, we fitted the measured primary spectrum with a mixture of predicted spectra for the decay modes $B \to De\nu$, $B \to D^*e\nu$, $B \to D^{**}e\nu$, $B \to DXe\nu$, and charmless decays $B \to X_u e\nu$. All spectra were obtained from full GEANT [34] simulations of $B\bar{B}$ events and included electroweak radiative corrections as described by the PHOTOS algorithm [35]. The decays $B \to D^*e\nu$ were generated according to HQET with CLEO-measured form-factor parameters [25]. $B \to De\nu$ decays were generated with the ISGW2 [26] model, and then reweighted to correspond to HQET with the form factor ρ^2 as measured by CLEO [24]. These $B \to De\nu$ and $B \to D^*e\nu$ components of the fit were constrained to be within $\pm 2\sigma$ of the measured exclusive branching fractions [28]. The third fit component, denoted $B \to D^{**}e\nu$, represented a mixture of decays to higher-mass charmed mesons as described by ISGW2 [26]. The fourth component was nonresonant $B \to DXe\nu$ as described by the model of Goity and Roberts [27]. These last two were constrained in the fit only to the extent that they were not allowed to be negative. The final component was the charmless decays $B \to X_u \ell\nu$ modeled with a hybrid inclusive/exclusive generator developed by CLEO. This model was built on the inclusive description of $B \to X_u \ell\nu$ developed by DeFazio and Neubert [36], with shape-function parameters determined by fitting CLEO's inclusively measured $B \to X_s\gamma$ energy spectrum [14]. For all final states with hadronic masses up to that of the $\rho(1450)$, exclusive final states, as described by the ISGW2 model [26], were substituted. The normalization of the $B \to X_u e\nu$ component was fixed by the partial branching fraction in the 2.2-2.6 GeV/c momentum region measured by CLEO [37].

The fit performed over $0.6 < p_e < 2.6$ GeV/c according to these specifications gave a χ^2 of 34.5 for 38 degrees of freedom, although it is noteworthy that the $B \to De\nu$ and $B \to D^*e\nu$ branching fractions were pinned at their $+2\sigma$ limits. For this fit the fraction of

the semileptonic decay spectrum below 600 MeV/c was 0.064.

We assessed the systematic uncertainty in this estimate by performing a large number of variations of the standard fit. In each case we refitted with only one ingredient changed. The difference between the standard value for the spectral fraction and that for the modified fit was recorded as the systematic uncertainty associated with that ingredient, and the overall systematic uncertainty was obtained by combining in quadrature.

The variations considered included $\pm 1\sigma$ variations in the form-factor parameters for $B \to De\nu$ and $B \to D^* e\nu$, extreme variations in the rates of the less well known D^{**} and nonresonant components, variations in the normalization of the fixed $B \to X_u e\nu$ component, a 30% variation in the electroweak radiative corrections applied to the spectra (the approximate difference between PHOTOS and the calculation of Atwood and Marciano [38]), and variations in the momentum scale with which B-decay distributions were boosted into the lab frame.

A persistent feature of the fits in the above list was that they demanded branching fractions for $B \to De\nu$ and $B \to D^* e\nu$ that were not in good agreement with world-average values [28]. To address this we also fitted the spectrum with the $B \to De\nu$ and $B \to D^* e\nu$ branching fractions fixed to their PDG 2002 values, with the other $B \to X_c e\nu$ components left free. The result was a very poor fit to the spectrum (χ^2=85.5/38 d.o.f) and an undetected spectral fraction of 0.070. Even though this case was strongly disfavored by the measured electron spectrum, we included it in assessing the systematic uncertainty.

Dividing the measured partial branching by the above-determined fraction of the B semileptonic momentum spectrum above 0.6 GeV/c of 0.936 ± 0.006 gives the total B semileptonic branching ratio:

$$\mathcal{B}(B \to Xe\nu) = (10.91 \pm 0.09 \pm 0.24)\%. \tag{5}$$

The first uncertainty is statistical and the second is systematic. The computation of the systematic uncertainty is broken down in Table III.

Source	$\Delta\mathcal{B}_{SL}(\%)$
J/ψ	0.003
π^0	0.006
γ	0.023
Same B secondaries	0.052
Upper Vertex D_s	0.091
Upper Vertex D	0.065
τ	0.041
$\psi(2S)$	0.005
Other Backgrounds	0.003
Tags from Secondaries	0.014
Electron Identification	0.113
Mixing Parameter	0.035
Continuum Subtraction	0.028
Track Quality Efficiency	0.001
Diagonal Cut Efficiency	0.008
Veto Efficiency	0.006
Muon Fake Rate	0.001
$\Delta(p)$	0.021
Event Selection Ratio	0.128
Fit Extrapolation	0.078
Total	0.236

TABLE III: Breakdown of systematic errors on $\mathcal{B}_{SL}$.

VII. MOMENTS OF THE ELECTRON-ENERGY DISTRIBUTION

Following the notation of Bauer *et al.* [18], we define the electron-energy moments as follows:

$$R[n, E_{\ell_1}, m, E_{\ell_2}] = \frac{\int_{E_{\ell_1}}^{E_\ell^{max}} E_\ell^n \frac{d\Gamma}{dE_\ell} dE_\ell}{\int_{E_{\ell_2}}^{E_\ell^{max}} E_\ell^m \frac{d\Gamma}{dE_\ell} dE_\ell}, \tag{6}$$

where $E_\ell^{max} = 2.5$ GeV. For convenience, we denote $R[1, E_{min}, 0, E_{min}]$ and $R[2, E_{min}, 0, E_{min}]$, as $\langle E_\ell \rangle$ and $\langle E_\ell^2 \rangle$, with E_{min} (in GeV) as a subscript when necessary. We also use the spread of the spectrum, $\langle E_\ell^2 - \langle E_\ell \rangle^2 \rangle$ as an alternative to the second moment, as it is less strongly correlated with $\langle E_\ell \rangle$ than $\langle E_\ell^2 \rangle$.

The moments computed theoretically are for the "heavy-to-heavy" decay $B \to X_c \ell \nu$, while our spectrum and branching fraction measurements included all semileptonic decays. Before computing the energy moments we therefore subtracted the small contribution of $B \to X_u \ell \nu$ decays. The momentum spectrum for these decays was generated with the hybrid inclusive/exclusive model described in Sec. VI and the normalization was obtained from the CLEO inclusive end-point measurement [37]. To assess the systematic uncertainty associated with this subtraction, we varied both the normalization and the shape of the $B \to X_u \ell \nu$ component. CLEO's inclusive and exclusive [39] $B \to X_u \ell \nu$ measurements have shown that the proportion of the end-point ($2.2 - 2.6$ GeV/c) spectrum that is due to $B \to \pi/\rho/\eta/\omega \ell \nu$ is approximately 55%. This has been used for the central value in the hybrid model, and variations of $\pm 30\%$ in the exclusive component were used to assess the sensitivity to the spectral shape. The normalization was varied up and down by one standard deviation, using the combined statistical and systematic uncertainty of the end-point measurement.

After subtracting the $B \to X_u \ell \nu$ from the spectrum of Fig. 6, we obtained the final $B \to X_c \ell \nu$ spectrum shown in Fig. 7. From this spectrum we computed "raw" moments by direct integration. These moments required two corrections before they could be interpreted with the theoretical expressions. Because our moments were measured in the $\Upsilon(4S)$ rest frame, it was necessary to correct for the boost of the spectrum from the B rest frame, where theoretical predictions are calculated. This is a very straightforward incorporation of the approximately 300 MeV/c momentum of B mesons produced from an $\Upsilon(4S)$ decay at rest. It could be done quite well analytically, although we performed it using Monte Carlo simulations that included the precise beam-energy distribution of our data sample. Using Monte Carlo samples, the value of each moment was computed in the B and $\Upsilon(4S)$ rest frames and the difference was taken as an additive correction to be applied to the moment. The sensitivity to the momentum scale was explored by reweighting the spectra in B momentum and recomputing. The sensitivity to decay mode and model was shown to be negligible. For $\langle E_\ell \rangle_{0.6}$ this correction is (-2.4 ± 0.2) MeV.

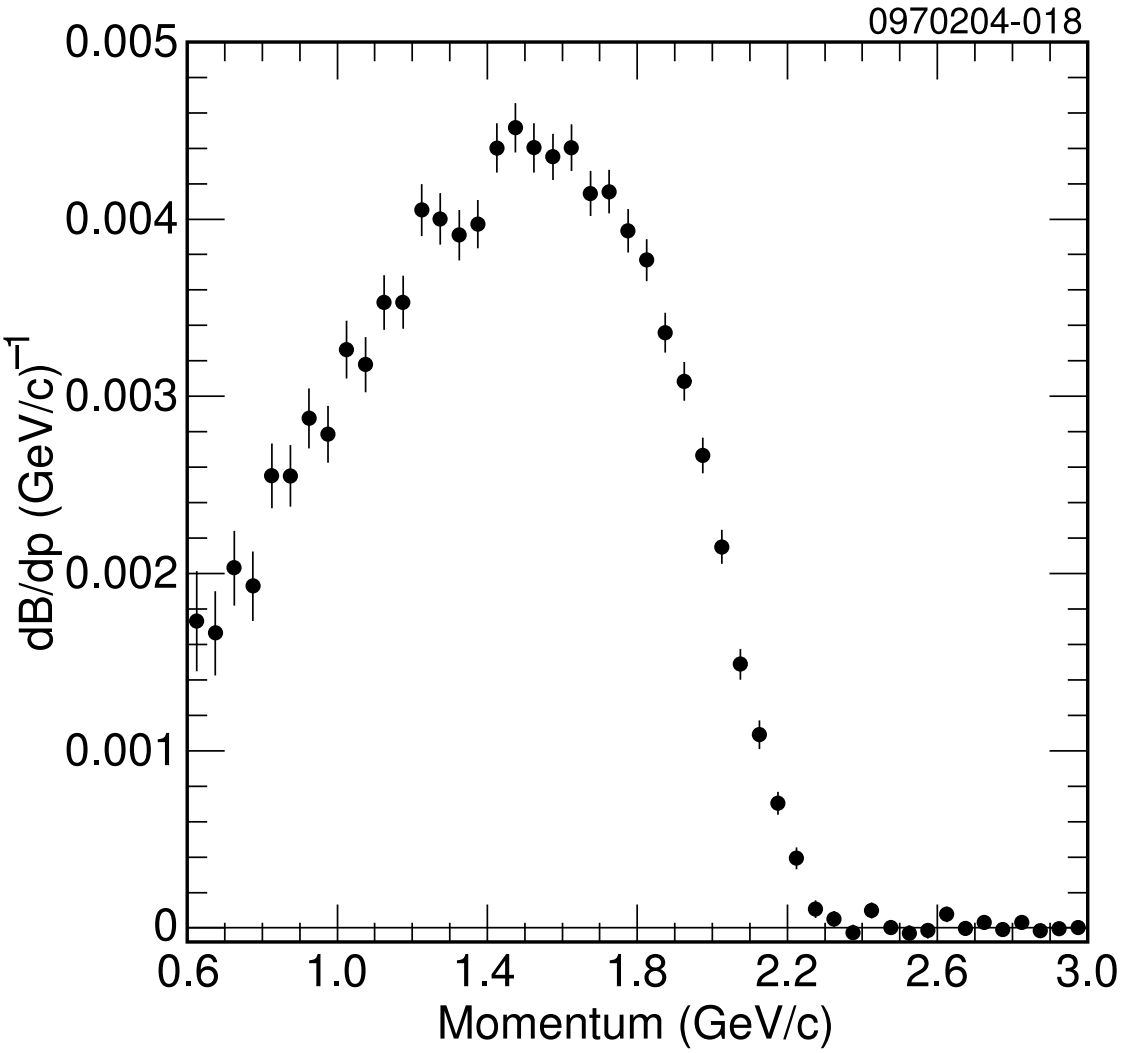

FIG. 7: The final $B \to X_c \ell \nu$ spectrum.

The second correction was for electroweak final-state radiation, which is not generally included in the theoretical expressions. Again, an additive correction was obtained, in this case using the PHOTOS algorithm [35] to generate spectra for different modes and models and computing the differences in moment values with and without the correction. For comparison and assessment of the systematic uncertainty associated with this correction, we also used the calculation of Atwood and Marciano [38]. The systematic uncertainty due to the electroweak correction was taken to be the difference between Atwood and Marciano and PHOTOS. For $\langle E_\ell \rangle_{0.6}$ this correction is $(+16.8 \pm 6.0)$ MeV. This is the largest systematic error in the moments measurement.

From our final spectrum, and after the two corrections described above were applied, we

E_{min}	$\langle E_\ell \rangle$ **(GeV)**	$\langle E_\ell^2 \rangle$ **(GeV^2)**	$\langle E_\ell^2 - \langle E_\ell \rangle^2 \rangle$ **(GeV^2)**
0.6	$1.4261 \pm 0.0043 \pm 0.0105$	$2.1856 \pm 0.0112 \pm 0.0271$	$0.1526 \pm 0.0021 \pm 0.0031$
0.7	$1.4509 \pm 0.0035 \pm 0.0079$	$2.2419 \pm 0.0097 \pm 0.0216$	$0.1374 \pm 0.0015 \pm 0.0018$
0.8	$1.4779 \pm 0.0031 \pm 0.0061$	$2.3066 \pm 0.0090 \pm 0.0177$	$0.1228 \pm 0.0013 \pm 0.0012$
0.9	$1.5119 \pm 0.0028 \pm 0.0047$	$2.3923 \pm 0.0085 \pm 0.0144$	$0.1068 \pm 0.0011 \pm 0.0010$
1.0	$1.5483 \pm 0.0026 \pm 0.0039$	$2.4890 \pm 0.0082 \pm 0.0127$	$0.0918 \pm 0.0010 \pm 0.0011$
1.1	$1.5884 \pm 0.0024 \pm 0.0033$	$2.6003 \pm 0.0080 \pm 0.0111$	$0.0775 \pm 0.0009 \pm 0.0012$
1.2	$1.6315 \pm 0.0023 \pm 0.0031$	$2.7259 \pm 0.0078 \pm 0.0109$	$0.0642 \pm 0.0009 \pm 0.0012$
1.3	$1.6794 \pm 0.0022 \pm 0.0029$	$2.8720 \pm 0.0078 \pm 0.0106$	$0.0516 \pm 0.0008 \pm 0.0011$
1.4	$1.7256 \pm 0.0021 \pm 0.0030$	$3.0192 \pm 0.0079 \pm 0.0112$	$0.0413 \pm 0.0008 \pm 0.0010$
1.5	$1.7792 \pm 0.0021 \pm 0.0027$	$3.1972 \pm 0.0081 \pm 0.0107$	$0.0316 \pm 0.0008 \pm 0.0010$

TABLE IV: Electron-energy moments for various minimum lepton-energy cuts E_{min}.

obtained values for electron-energy moments with minimum energies between 0.6 GeV and 1.5 GeV. These are given in Table IV. Note that these numbers are highly correlated. As a cross-check of our procedure for extracting the moments, we also computed them from the $B \to X_c \ell \nu$ spectra obtained with the fits to Monte Carlo-predicted spectra as described in Sec. VI. Consistent results were obtained in all cases.

Systematic uncertainties in the moment values were assessed with the techniques described in Sec. V (background and efficiency corrections) and earlier in this section (moment extraction). To provide a concrete illustration, the mean energy for the full measured spectrum is $\langle E_\ell \rangle_{0.6} = (1.4261 \pm 0.0043 \pm 0.0105)$ GeV, where the first error is statistical and the second is systematic. The largest sources of systematic uncertainty for this moment are the electroweak radiative correction (± 0.0060), upper-vertex charm background correction (± 0.0059), and electron identification (± 0.0046). All of these, and the total systematic uncertainty, diminish with increasing minimum-energy cut, as shown in Table IV.

VIII. INTERPRETATION AND CONCLUSIONS

In this paper we have presented a new measurement of the inclusive momentum spectrum for semileptonic B-meson decays using events with a high-momentum lepton tag and a sig-

nal electron in the full data sample collected with the CLEO II detector. Improvements in the understanding of background processes and optimized electron-identification procedures have resulted in significant improvements in systematic uncertainties relative to the previous CLEO measurement [3], which this analysis supersedes. We have used the normalization of the measured spectrum and an extrapolation for $0 < E_\ell < 0.6$ GeV based on a detailed model calculation constrained by data to obtain a new measurement of the B semileptonic branching fraction, $\mathcal{B}(B \to Xe\nu) = (10.91 \pm 0.09 \pm 0.24)\%$. This result is in excellent agreement with other recent measurements at the $\Upsilon(4S)$ [4, 5] and has better overall precision. These results have diminished the level of disagreement between measurements made at the $\Upsilon(4S)$ and those from Z^0 decays [2]. While still somewhat lower than theoretical predictions, the measured B semileptonic branching fraction is now less in conflict [1] with them than was previously the case.

We have also used our measured spectrum to determine the moments of electron energy in semileptonic B decays with minimum energies ranging from 0.6 GeV to 1.5 GeV (Table IV). Our measured value for the mean energy with $E_{min} = 1.5$ GeV/c, $\langle E_\ell \rangle_{1.5} = (1.7792 \pm 0.0021 \pm 0.0026)$ GeV, is in good agreement with the previous CLEO measurement of this quantity [40], $(1.7810 \pm 0.0007 \pm 0.0009)$ GeV. The earlier measurement was more precise because it used the entire inclusive spectrum for semileptonic B decays, without a lepton-tag requirement. That technique does not allow for measurements with smaller values of E_{min}, however, because of the large contribution of secondary charm decays. While electron-energy moments were not presented for the previous CLEO lepton-tagged measurement of $\mathcal{B}(B \to Xe\nu)$ [3], we note that moment values computed from fits to that spectrum are consistent with the current measurements.

Measurements of moments of different quantities and with sensitivity to different regions of phase space provide an ideal opportunity to test the description of inclusive B decays provided by the HQET/OPE methodology. Using this approach, theorists have derived expressions [18] for many inclusive properties of B decays, including the moments of the lepton energy and recoil hadronic mass in $B \to X_c \ell \nu$ and of the photon energy in $B \to X_s \gamma$. The physical observables are expressed as expansions in Λ_{QCD}/M_B and new parameters emerge at each order: $\bar{\Lambda}$ at order Λ_{QCD}/M_B, λ_1 and λ_2 at order Λ^2_{QCD}/M^2_B, and six parameters (ρ_1, ρ_2, $\mathcal{T}_1$, $\mathcal{T}_2$, $\mathcal{T}_3$, $\mathcal{T}_4$) at order Λ^3_{QCD}/M^3_B [41].

Previous CLEO moments measurements [14, 15, 40] have been interpreted with the-

oretical expansions in the pole-mass scheme to order $\beta_0(\alpha_s/\pi)^2$ in the perturbative and Λ^3_{QCD}/M^3_B in the nonperturbative expansion. The six third-order parameters were fixed in fitting the data, and fluctuated within bounds determined by dimensional arguments [41] for assessment of the uncertainty. A combined fit to the data gave $\bar{\Lambda} = (0.39 \pm 0.14)$ GeV and $\lambda_1 = (-0.25 \pm 0.15)$ GeV^2, where the uncertainties are dominated by theory [40].

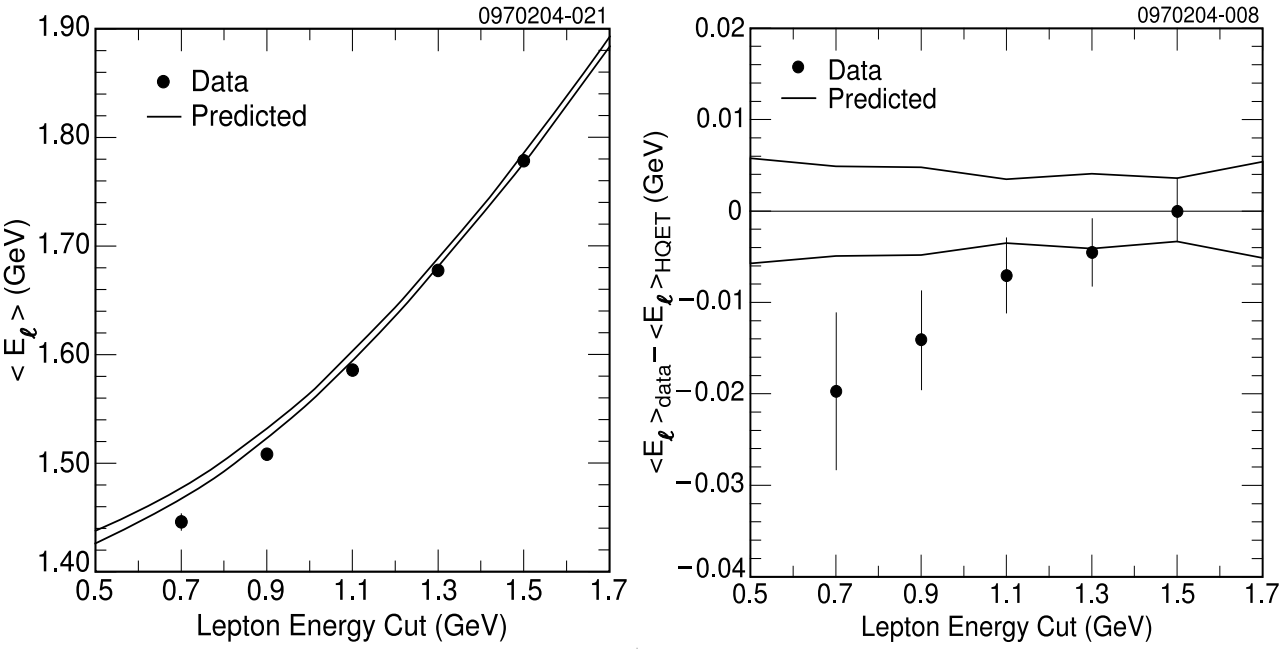

FIG. 8: **Left:** $\langle E_\ell \rangle$ as a function of E_{min}. The points are data and the band is the $\pm 1\sigma$ prediction in the pole-mass scheme [18]. **Right:** $\langle E_\ell \rangle_{data} - \langle E_\ell \rangle_{HQET}$ as a function of E_{min}. The points are the data from Table IV and the band is the $\pm 1\sigma$ prediction in the pole-mass scheme. Inputs for these plots were set by the first photon energy moment of $b \to s\gamma$ [14] and $\langle E_\ell \rangle_{1.5}$.

The plots in Fig. 8 show our measured values of $\langle E_\ell \rangle$ as a function of the minimum lepton energy cut and the HQET/OPE predictions for the electron-energy moments in the pole mass scheme provided by [18]. The plot on the left shows the measurements and the prediction, while the plot on the right shows the difference between the measurements and the prediction. The values for $\bar{\Lambda}$ and λ_1 are constrained by the first photon-energy moment of the $b \to s\gamma$ spectrum [14] and our measurement of $\langle E_\ell \rangle_{1.5}$. The third-order parameters $\mathcal{T}_{1-4}$ were taken to be to $(0 \pm 0.5$ GeV$)^3$. The parameter ρ_1 was taken to be (0.0625 ± 0.0625) GeV^3 [41], and ρ_2 is constrained by $B^* - B$ and $D^* - D$ mass splittings [18]. The error bars on the data points represent the combined statistical and systematic uncertainties of the measurements. There is substantial correlation among the data values for the different E_{min} cases. The

width of the band is set by the uncertainty in the measurements of $\bar{\Lambda}$ and λ_1, variation of the third-order expansion parameters, and variation of the perturbative QCD corrections.

As can be seen in Fig. 8, there is an increasing disagreement as E_{min} is reduced between the measured mean energy and the value extrapolated with HQET. We note again that these results have been obtained by using the PHOTOS algorithm [35] to correct for final-state radiation. There is considerable uncertainty in this correction, and if the prescription of Atwood and Marciano [38] were instead used, the disagreement between our measurement and the HQET computation would be increased by 25%. The difference between these two computations is the largest contribution to the systematic uncertainty in the measurement of the mean energy.

Fig. 9 shows four bands in the $\bar{\Lambda} - \lambda_1$ space. Along with the standard bands for $\langle E_\ell \rangle_{0.7}$ and $(\langle E_\ell^2 - \langle E_\ell \rangle^2 \rangle)_{0.7}$, we show bands for the difference of the mean $\langle E_\ell \rangle_{1.5} - \langle E_\ell \rangle_{0.7}$ and the difference in the variance $(\langle E_\ell^2 - \langle E_\ell \rangle^2 \rangle)_{0.7} - (\langle E_\ell^2 - \langle E_\ell \rangle^2 \rangle)_{1.5}$ to isolate the information that is independent of the measurements of the moments with $E_\ell > 1.5$ GeV. The width of the bands indicates the combined experimental and theoretical uncertainties. As can be seen, the variance (band 2) and the difference in the variances (band 4) are compatible with other measurements [40], whereas the difference in the means (band 3) is the predominant source of disagreement between data and theory.

There are several possible explanations for the observed inconsistency within HQET of the parameters extracted from our different energy-moment measurements. In light of the sizable disagreement between the PHOTOS and Atwood/Marciano treatments of electroweak radiation, we cannot exclude an error in this correction that is outside of the quoted systematic uncertainty, although it seems unlikely. Possible theoretical explanations include problems with the specific HQET/OPE implementations that we have used, incorrect assumptions about the unknown third-order parameters, and problems with the underlying assumptions, such as quark-hadron duality. A comprehensive fit, including correlations, of all published CLEO moments [14, 15, 40], the electron-energy moments in this paper, and new measurements of the recoil hadronic mass moments in $B \to X_c \ell \nu$ [21] is currently in preparation. By leaving parameters free at third order, this will determine if any of the HQET/OPE formulations, including the different mass schemes presented by Bauer *et al.* [18] and the kinetic mass scheme of Uraltsev *et al.* [42], can accommodate all of the data.

During the final preparation of this paper, we learned of a preprint from the BaBar

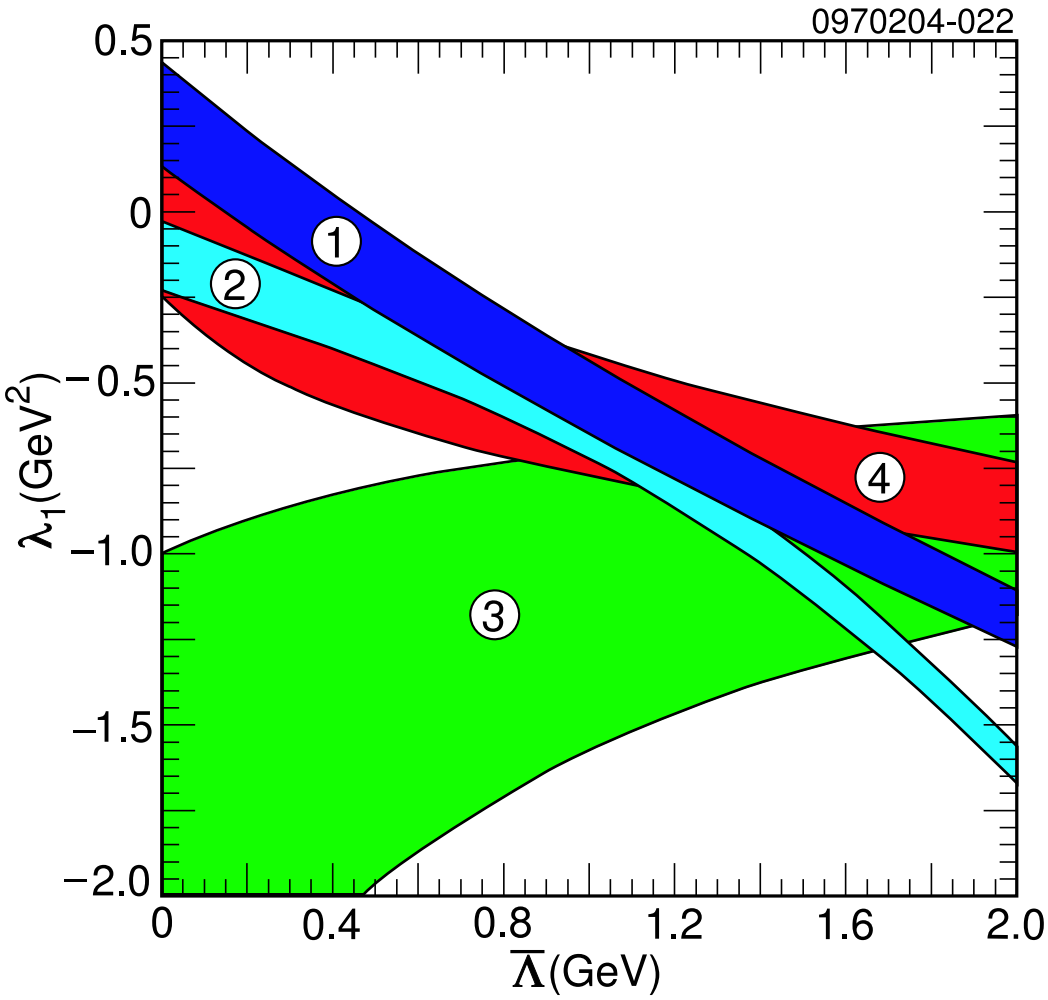

FIG. 9: Bands in the $\bar{\Lambda} - \lambda_1$ plane from $\langle E_\ell \rangle$ with $E_\ell > 0.7$ GeV (band 1), $\langle E_\ell^2 - \langle E_\ell \rangle^2 \rangle$ with $E_\ell > 0.7$ GeV (band 2), $\langle E_\ell \rangle_{1.5} - \langle E_\ell \rangle_{0.7}$ (band 3), and $(\langle E_\ell^2 - \langle E_\ell \rangle^2 \rangle)_{0.7} - (\langle E_\ell^2 - \langle E_\ell \rangle^2 \rangle)_{1.5}$ (band 4). The widths of the bands reflect the combined experimental and theoretical 1σ uncertainties. These bands were calculated in the pole mass scheme [18].

collaboration reporting new measurements of the moments of the electron-energy spectrum in semileptonic B decays [43]. The BaBar results are based on an $\Upsilon(4S)$ sample with about five times the integrated luminosity of our CLEO II data and are consistent within quoted uncertainties with the measurements reported in this paper. The combined statistical and systematic uncertainties of the BaBar results range from essentially identical to those of our measurements (partial semileptonic branching fraction) to approximately two thirds as large (first energy moments).

IX. ACKNOWLEDGMENTS

We gratefully acknowledge the efforts of the CESR staff in providing our excellent data sample. We thank C. Bauer, N. Uraltsev, A. Vainshtein, M. Voloshin, and P. Gambino for their useful discussions and correspondence. This work was supported by the National Science Foundation, the U.S. Department of Energy, the Research Corporation, and the Texas Advanced Research Program.

---

[1] I. I. Y. Bigi, B. Blok, M. A. Shifman, and A. I. Vainshtein, Phys. Lett. **B323**, 408 (1994), arXiv:hep-ph/9311339.

[2] H. Albrecht et al. (ARGUS Collaboration), Phys. Lett. **B318**, 397 (1993).

[3] B. Barish et al. (CLEO Collaboration), Phys. Rev. Lett. **76**, 1570 (1996).

[4] B. Aubert et al. (BABAR Collaboration), Phys. Rev. **D67**, 031101 (2003), arXiv:hep-ex/0208018.

[5] K. Abe et al. (BELLE Collaboration), Phys. Lett. **B547**, 181 (2002), arXiv:hep-ex/0208033.

[6] M. A. Shifman and M. B. Voloshin, Sov. J. Nucl. Phys. **41**, 120 (1985).

[7] J. Chay, H. Georgi, and B. Grinstein, Phys. Lett. **B247**, 399 (1990).

[8] I. I. Y. Bigi, N. G. Uraltsev, and A. I. Vainshtein, Phys. Lett. **B293**, 430 (1992), arXiv:hep-ph/9207214.

[9] I. I. Y. Bigi, M. A. Shifman, N. G. Uraltsev, and A. I. Vainshtein, Phys. Rev. Lett. **71**, 496 (1993), arXiv:hep-ph/9304225.

[10] K. Adel and Y.-P. Yao, Phys. Rev. **D49**, 4945 (1994), arXiv:hep-ph/9308349.

[11] M. B. Voloshin, Phys. Rev. **D51**, 4934 (1995), arXiv:hep-ph/9411296.

[12] M. Gremm, A. Kapustin, Z. Ligeti, and M. B. Wise, Phys. Rev. Lett. **77**, 20 (1996), arXiv:hep-ph/9603314.

[13] M. Neubert, Phys. Rev. **D49**, 4623 (1994), arXiv:hep-ph/9312311.

[14] S. Chen et al. (CLEO Collaboration), Phys. Rev. Lett. **87**, 251807 (2001), arXiv:hep-ex/0108032.

[15] D. Cronin-Hennessy et al. (CLEO Collaboration), Phys. Rev. Lett. **87**, 251808 (2001), arXiv:hep-ex/0108033.

[16] M. Calvi (DELPHI Collaboration) (2002), arXiv:hep-ex/0210046.

[17] M. Battaglia et al., ECONF **C0304052**, WG102 (2003), arXiv:hep-ph/0210319.

[18] C. W. Bauer, Z. Ligeti, M. Luke, and A. V. Manohar (2002), arXiv:hep-ph/0210027.

[19] P. Tipton, Ph.D. thesis, University of Rochester (1987).

[20] CLEO collaboration, in preparation.

[21] S. E. Csorna et al. (CLEO Collaboration), submitted to Physical Review D, arXiv:hep-ex/0403052.

[22] Y. Kubota et al. (CLEO Collaboration), Nucl. Instrum. Meth. **A320**, 66 (1992).

[23] T. S. Hill, Nucl. Instrum. Meth. **A418**, 32 (1998).

[24] M. Athanas et al. (CLEO Collaboration), Phys. Rev. Lett. **79**, 2208 (1997), arXiv:hep-ex/9705019.

[25] J. E. Duboscq et al. (CLEO Collaboration), Phys. Rev. Lett. **76**, 3898 (1996).

[26] D. Scora and N. Isgur, Phys. Rev. **D52**, 2783 (1995), arXiv:hep-ph/9503486.

[27] J. L. Goity and W. Roberts, Phys. Rev. **D51**, 3459 (1995), arXiv:hep-ph/9406236.

[28] K. Hagiwara et al. (Particle Data Group), Phys. Rev. **D66**, 010001 (2002).

[29] J. P. Alexander et al. (CLEO Collaboration), Phys. Rev. Lett. **86**, 2737 (2001).

[30] R. Wang, Ph.D. thesis, University of Minnesota (1994).

[31] C. Stepaniak, Ph.D. thesis, University of Minnesota (2004).

[32] S. Anderson et al. (CLEO Collaboration) (2002), arXiv:hep-ex/0207059.

[33] D. Abbaneo et al. (The LEP Electroweak Working Group), Report No. CERN-EP/2001-50.

[34] R. Brun et al., *Geant 3.15* (1987), CERN Report No. DD/EE/84-1.

[35] E. Barberio and Z. Was, Comput. Phys. Commun. **79**, 291 (1994).

[36] F. D. Fazio and M. Neubert, JHEP **9906**, 017 (1999), arXiv:hep-ph/9905351.

[37] A. Bornheim et al. (CLEO Collaboration), Phys. Rev. Lett. **88**, 231803 (2002), arXiv:hep-ex/0202019.

[38] D. Atwood and W. J. Marciano, Phys. Rev. D **D41**, 1736 (1990).

[39] S. B. Athar et al. (CLEO Collaboration), Phys. Rev. **D68**, 072003 (2003), arXiv:hep-ex/0304019.

[40] A. H. Mahmood et al. (CLEO Collaboration), Phys. Rev. **D67**, 072001 (2003), arXiv:hep-ex/0212051.

[41] M. Gremm and A. Kapustin, Phys. Rev. **D55**, 6924 (1997), arXiv:hep-ph/9603448.

[42] P. Gambino and N. Uraltsev (2004), arXiv:hep-ph/0401063.

[43] B. Aubert et al. (BABAR Collaboration) (2004), arXiv:hep-ex/0403030.